Software News and Update
A Flexible Implementation of Frozen-Density Embedding for Use in Multilevel Simulations

CHRISTOPH R. JACOB,[1] JOHANNES NEUGEBAUER,[2] LUCAS VISSCHER[1]
[1]*Department of Theoretical Chemistry, Faculty of Sciences, Vrije Universiteit Amsterdam, De Boelelaan 1083, 1081 HV Amsterdam, The Netherlands*
[2]*ETH Zurich, Laboratorium für Physikalische Chemie, Wolfgang-Pauli-Strasse 10, 8093 Zurich, Switzerland*

Received 9 July 2007; Revised 14 September 2007; Accepted 23 September 2007
DOI 10.1002/jcc.20861
Published online 6 November 2007 in Wiley InterScience (www.interscience.wiley.com).

Abstract: A new implementation of frozen-density embedding (FDE) in the Amsterdam Density Functional (ADF) program package is presented. FDE is based on a subsystem formulation of density-functional theory (DFT), in which a large system is assembled from an arbitrary number of subsystems, which are coupled by an effective embedding potential. The new implementation allows both an optimization of all subsystems as a linear-scaling alternative to a conventional DFT treatment, the calculation of one active fragment in the presence of a frozen environment, and intermediate setups, in which individual subsystems are fully optimized, partially optimized, or completely frozen. It is shown how this flexible setup can facilitate the application of FDE in multilevel simulations.

 J Comput Chem 29: 1011–1018, 2008

Key words: frozen-density embedding; density-functional theory; ADF; multilevel methods; QM/QM methods

Introduction

Applications of quantum chemical methods for studying biological systems often require the use of multilevel methods, i.e., methods that treat different parts of the total system using different approximations (for recent examples, see, e.g., refs. 1–4). In particular, QM/QM methods[5] [i.e., multilevel methods that apply different quantum mechanical (QM) methods in different regions], and QM/MM methods[6–8] [i.e., methods that combine a QM treatment with a molecular mechanics (MM) treatment] are widely used.

Different multilevel methods can be classified according to the way in which the interaction between the different levels is described.[9] Many methods, in particular QM/QM methods, only employ what is usually referred to as mechanical coupling, i.e., the coupling between the different regions is only described at the level of the total energy.[5,10–12] In these methods, no effect of the other region is included in the potential, so that only an indirect effect on molecular properties due to changes in the equilibrium structure can be described. In contrast, most standard QM/MM methods[8,13,14] include the electrostatic potential of the MM environment in the QM calculation (electronic coupling), thus allowing a more adequate description of molecular properties. An even more accurate description of the coupling can be obtained by also considering the polarization of the MM environment due to the QM part, as it is done in some advanced QM/MM schemes that employ polarizable force fields.[15–17]

However, QM/MM methods rely on a careful parametrization of the MM part, and even though there are accurate force fields available for many classes of compounds, these often cannot be applied for nonstandard system, such as compounds containing transition metal atoms. On the other hand, common QM/QM methods do not suffer from these restrictions, but they are limited to describing the interaction between the different regions at the level of mechanical coupling only.

One promising multilevel method is the frozen-density embedding (FDE) scheme within density-functional theory (DFT) first developed by Wesolowski and Warshel.[18,19] It describes the full system on a QM basis and at the same time includes the electronic coupling between different regions. Even though the FDE scheme relies on the use of an approximate kinetic-energy functional, it offers a treatment that is in principle exact. It has been successfully

Correspondence to: C. R. Jacob; e-mail: jacob@few.vu.nl

Contract/grant sponsors: The Netherlands Organization for Scientific Research (NWO), Liebig-Stipendium of the Fonds der Chemischen Industrie

applied in a number of studies, e.g., of solvent effects on absorption spectra,[20–22] electron spin resonance (ESR) parameters[23] and nuclear magnetic resonance (NMR) chemical shifts.[24] It has further been employed for describing induced circular dichroism in host–guest systems[25] and for free-energy calculations in protein environments.[4,26]

In the subsystem formulation of DFT,[27] which forms the starting point for FDE, the total system is partitioned into N subsystems, and the total electron density $\rho_{\mathrm{tot}}(\boldsymbol{r})$ is represented as the sum of the electron densities of these fragments $\rho_i(\boldsymbol{r})$ $(i = 1, \ldots, N)$. Given this partitioning of the electron density, the DFT total energy can be expressed as a functional of the subsystem densities.

$$\begin{aligned} E[\rho_1, \ldots, \rho_N] = & \int \rho_{\mathrm{tot}}(\boldsymbol{r}) \left(\sum_{i=1}^{N} v_i^{\mathrm{nuc}}(\boldsymbol{r}) \right) d\boldsymbol{r} \\ & + \frac{1}{2} \int \frac{\rho_{\mathrm{tot}}(\boldsymbol{r}) \rho_{\mathrm{tot}}(\boldsymbol{r}')}{|\boldsymbol{r} - \boldsymbol{r}'|} d\boldsymbol{r} d\boldsymbol{r}' \\ & + E_{\mathrm{xc}}[\rho_{\mathrm{tot}}] + \sum_{i=1}^{N} T_{\mathrm{s}}[\rho_i] + T_{\mathrm{s}}^{\mathrm{nadd}}[\rho_1, \ldots, \rho_N], \end{aligned} \tag{1}$$

where $\rho_{\mathrm{tot}} = \sum_{i=1}^{N} \rho_i$ is the total electron density, v_i^{nuc} is the electrostatic potential of the nuclei in subsystem i, E_{xc} is the exchange-correlation functional, and $T_{\mathrm{s}}^{\mathrm{nadd}}[\rho_1, \ldots, \rho_i]$ is the nonadditive kinetic-energy functional, which is defined as

$$T_{\mathrm{s}}^{\mathrm{nadd}}[\rho_1, \ldots, \rho_N] = T_{\mathrm{s}}[\rho_{\mathrm{tot}}] - \sum_{i=1}^{N} T_{\mathrm{s}}[\rho_i]. \tag{2}$$

In these expressions, $T_{\mathrm{s}}[\rho]$ is the kinetic energy of the noninteracting reference system, as it is defined within Kohn–Sham (KS) DFT, which is usually calculated using the KS orbitals. However, with the given partitioning into subsystems, KS orbitals are only available for the subsystems and not for the full system, and $T_{\mathrm{s}}[\rho_{\mathrm{tot}}]$ can therefore not be calculated directly. For this reason, in practical applications an approximate kinetic energy functional has to be used to evaluate $T_{\mathrm{s}}^{\mathrm{nadd}}$. Most previous applications employ either the Thomas–Fermi (TF) kinetic energy functional or the GGA functional PW91k,[28] which have been shown to yield accurate results for weakly interacting and hydrogen-bound systems.[29,30] However, the applicability of these functionals is limited to cases in which the interaction between the subsystems is not too large, and the description of covalent bonds between subsystems is currently not possible. The development of improved approximate kinetic-energy functionals for the application in the FDE scheme is, therefore, an active area of research.[19,31]

The electron densities of the individual subsystem ρ_i can be determined by minimizing the above total energy functional with respect to the density of this subsystem, while keeping the densities of the other subsystems frozen. This leads to a set of coupled KS-like equations,

$$\left[-\frac{\nabla^2}{2} + v_{\mathrm{eff}}^{\mathrm{KS}}[\rho_i](\boldsymbol{r}) + v_{\mathrm{emb}}^{(\mathrm{i})}[\rho_1, \ldots, \rho_N](\boldsymbol{r}) \right] \phi_k^{(i)}(\boldsymbol{r}) = \epsilon_k^{(i)} \phi_k^{(i)}(\boldsymbol{r}) \tag{3}$$

from which the KS orbitals $\{\phi_k^{(i)}\}$ and the associated electron density ρ_i of the subsystem can be obtained. In this equation, $v_{\mathrm{eff}}^{\mathrm{KS}}[\rho_i]$ is the KS effective potential of the isolated subsystem i containing the usual terms of the nuclear potential, the Coulomb potential of the electron, and the exchange–correlation potential. The effective embedding potential $v_{\mathrm{emb}}^{(\mathrm{i})}[\rho_1, \ldots, \rho_N]$ contains the effect of the other subsystems on subsystem i and is given by

$$\begin{aligned} v_{\mathrm{emb}}^{(\mathrm{i})}[\rho_1, \ldots, \rho_N] = & \sum_{j \neq i} v_j^{\mathrm{nuc}}(\boldsymbol{r}) + \sum_{j \neq i} \int \frac{\rho_j(\boldsymbol{r}')}{|\boldsymbol{r} - \boldsymbol{r}'|} d\boldsymbol{r}' \\ & + \left. \frac{\delta E_{\mathrm{xc}}[\rho]}{\delta \rho} \right|_{\rho = \rho_{\mathrm{tot}}(\boldsymbol{r})} - \left. \frac{\delta E_{\mathrm{xc}}[\rho]}{\delta \rho} \right|_{\rho = \rho_i(\boldsymbol{r})} \\ & + \frac{\delta T_{\mathrm{s}}^{\mathrm{nadd}}[\rho_1, \ldots, \rho_N]}{\delta \rho_i(\boldsymbol{r})}. \end{aligned} \tag{4}$$

It contains the potential of the environment, the Coulomb potential of the electrons in the environment, a nonadditive exchange-correlation component, and a kinetic-energy component.

However, since the density of all the other subsystems appears in the embedding potential for one of the subsystems, the subsystem densities have to be determined iteratively.[27] One possibility of doing this is to employ "freeze-and-thaw" cycles,[32] i.e., to determine the electron density of one active subsystem, which is then frozen while the density of the next subsystem is determined. This procedure can be repeated multiple times for each subsystem, until the densities of all subsystems are converged. Alternatively, the orbitals of all subsystems can be determined simultaneously by constructing a block-diagonal Fock-matrix (consisting of one block for each subsystem) in each SCF iteration, i.e., in each SCF iteration the electron densities of all subsystems are updated.

This fully variational approach, in which the densities of all subsystems are optimized, can be used as an alternative to conventional KS-DFT calculation for large systems. By construction, it scales linearly with the number of subsystems. Initially, it has been applied by Cortona et al. for calculations on simple ionic crystals (e.g., alkali halides,[33] alkali-earth oxides,[34] and alkali-earth sulfides[35]), by determining the densities of the ions individually. While in the implementation of Cortona, these densities are constraint to be spherical, an extended scheme has been implemented by Mehl and coworkers. They allow deformations of the atomic densities, and studied alkali halides[36] and corundum.[37]

Recently, the fully variational subsystem DFT approach has been implemented by Iannuzzi et al. in the CP2K (refs. 38 and 39) program package.[40] With their implementation molecular dynamics simulations can be performed, in which the individual molecules are treated as subsystems. In this scheme all subsystems are treated on the same footing and the implementation is most efficient in the case of subsystems of the same kind, e.g., the molecules in a homogeneous liquid phase. Another implementation has been presented by Shimojo et al.[41] who also implemented this subsystem DFT scheme in combination with a numerical integration scheme employing hierarchical real-space grids as an efficient alternative

to standard KS-DFT calculations. They have applied their implementation to MD simulations of aluminum nanoparticles and of nanoindentation of ceramics materials.[42]

The presented subsystem formulation of DFT can also be employed as a method to model the effect of an environment by only optimizing the electron density of one active subsystem in the presence of a frozen environment density and by introducing additional approximations in the construction of this frozen density.[18,43] This strategy, usually referred to as FDE, has been applied in a number of studies of solvent effects on different molecular properties, in which the solvent was constructed as a superposition of the gas phase densities of the individual solvent molecules.[20–23]

It is particularly suited for studying molecular properties, which are often rather local and can be described well in terms of an active system (of which some property is calculated) and an environment. The theory presented earlier has been generalized to the calculation of a number of properties, like the calculation of electronic absorption spectra using time-dependent DFT (TDDFT)[44,45] and of NMR shieldings.[24] In these cases also the property calculation is sped up significantly compared with the treatment of the full system, because it only has to be performed for the much smaller active subsystem (which has been influenced by the environment).

The FDE scheme was implemented by Wesolowski and coworkers both in deMon and in deMon2k[46–48] as well as in the Amsterdam Density-Functional (ADF) program package.[21,49,50] Both implementations are limited to two subsystems, of which one is optimized while the other subsystem is kept frozen. In ADF, this frozen density can also be composed from the density of several fragments to obtain approximate environment densities. In both implementations, it is also possible to perform fully variational subsystem DFT calculations by exchanging the role of the frozen and the nonfrozen subsystem in freeze-and-thaw cycles, but this requires several runs of the program and is in general limited to two subsystems.

The implementation in ADF uses an efficient numerical integration scheme that makes it applicable also in the case of rather large (up to more than 1000 atoms) environments (see, e.g., ref. 21). Furthermore, ADF supports the generalization of FDE to TDDFT[44,51] and to the calculation of NMR parameters[24] and can therefore be applied for calculating a wide range of molecular properties (see, e.g., refs. 22, 23, 25).

In this article, we present a new, improved implementation of FDE in the ADF program package, based on the previous implementation of Wesolowski and coworkers. This new implementation is an intermediate between the two approaches described earlier, i.e., the fully variational subsystem DFT treatment and the FDE approach using an approximate environment. In our implementation the total system is composed of an arbitrary number of fragments that can each be treated using different levels of accuracy, while the interaction between the fragments is described by the embedding potential of eq. (4). On the one hand, the density of all subsystems can be fully optimized, leading to a subsystem DFT implementation similar to that of Hutter and coworkers.[40] On the other hand, it is also possible to optimize only the density of one active subsystem, while all other subsystems form a frozen environment, leading to the FDE scheme previously implemented in ADF. Furthermore, our implementation also allows all kinds of intermediate setup, e.g., a number of subsystems are fully optimized, while for other subsystems the gas-phase density is only polarized in one freeze-and-thaw cycle and while for the remaining subsystems the frozen density of the isolated molecule is used. In addition, a number of additional options can be specified for each fragment.

Implementation

Our implementation of FDE in the ADF program package makes use of the concept of fragments, that is central to many aspects of the ADF package.[50] In ADF, any system is build from fragments, which are either atoms or larger parts of the system under study. A lot of quantities calculated, in particular the bonding energy, are then expressed relative to these fragments, and a number of the analysis tools of ADF, like the energy decomposition analysis,[52] rely on the decomposition of the total system into the initial fragments.

This fragments setup has been extended by introducing frozen fragments as a new type of fragments. Similar to the usual nonfrozen fragments, for each frozen fragment the results of a previous ADF calculation have to be provided. In the simplest possible setup, only one frozen fragment is used. In this case, the nonfrozen subsystem will be build from all nonfrozen fragments, as it is normally done in ADF. The frozen fragment will be used as frozen density, and an embedding potential according to eq. (4) will be included in the calculation of the nonfrozen subsystem. This simple setup with only one frozen fragment is similar to the FDE implementation that was previously available in ADF.

In addition, our new implementation also allows the use of more than one frozen fragment. In this case, the frozen densities of all these frozen fragments are added when the embedding potential is constructed. This allows the use of frozen densities that are given by the sum of the densities of isolated molecules, as they are used in studies of solvent effects,[20,21] in a very simple way. If the frozen environment is composed of identical molecules and if the same geometry is used for these molecules, the density of the isolated molecules only has to be calculated once, and this density will be automatically rotated and translated so that it can be used for multiple frozen fragments.

For each fragment, a number of additional options can be specified. It is possible to choose whether the exact density (calculated using the molecular orbital coefficients) or the fitted density, which can be calculated more efficiently, should be used for the construction of the frozen density. Furthermore, it can be specified whether the basis functions of a frozen fragment are included in the calculation of the nonfrozen subsystem. This way it is easily possible to perform calculations using the so-called supermolecular basis set expansion, which is useful for benchmarking calculations.[30,32]

Our new implementation allows the efficient treatment of very large environments. In particular, it employs the numerical integration scheme described in ref. 21, which uses an integration grid that is centered on the nonfrozen subsystem and which does not increase in size for sufficiently large environments. Therefore, the computational effort for most parts of the calculation, like the self-consistent field (SCF) iterations or property calculations does not increase if the size of the environment is increased. Only the computational effort for the construction of the electrostatic part of the embedding potential and of the frozen electron density, which are both only

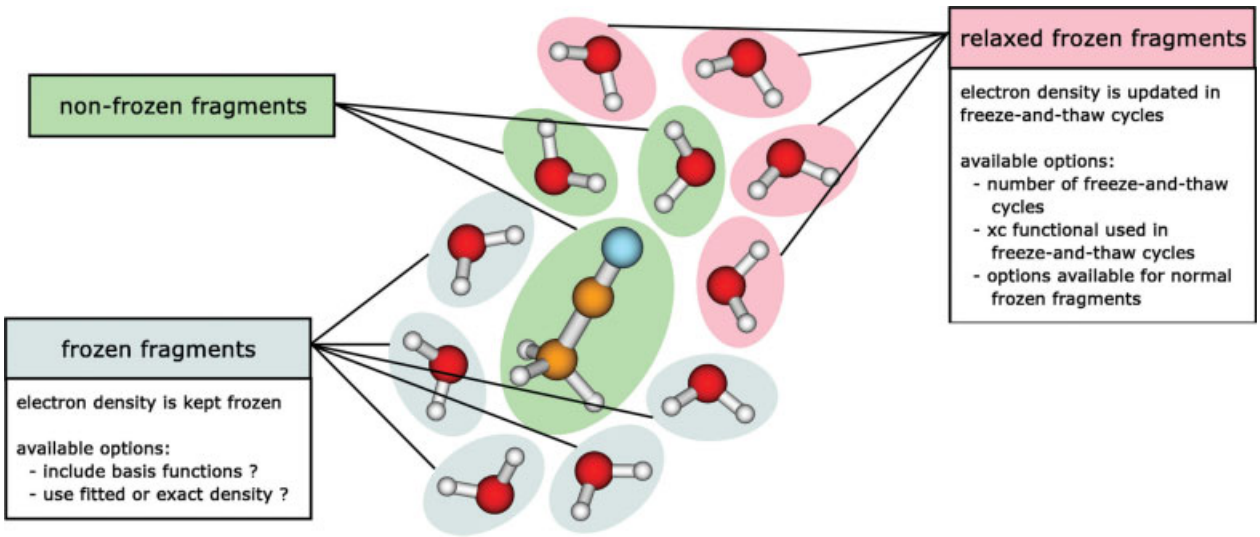

Figure 1. Schematic overview of the fragment-based implementation. The implementation support non-frozen fragments, normal frozen fragments, and frozen fragments for which the density is relaxed in freeze-and-thaw cycles. In addition, a number of options are available for each fragment.

done once at the beginning of the calculation, scales linearly with the size of the environment. Furthermore, the implementation is efficiently parallelized by applying ADF's parallelization techniques, in particular by distributing the grid points used for the numerical integration among the available nodes.

One of the major new features of our implementation is the ability to relax the electron density of individual frozen subsystems. For each frozen fragment, it is possible to specify whether its density should be relaxed. In this case, the electron density of this fragment will be calculated in a "freeze-and-thaw" cycle, i.e., the fragment is thawed, while all other fragments are frozen. This will be repeated for all frozen fragments for which the density should be relaxed. These relaxation steps are performed several times, until all densities are converged, or until a user-specified maximum number of freeze-and-thaw cycles has been reached. The computational efficiency of the implementation in the case of freeze-and-thaw cycles is ensured by constructing different numerical integration grids as described in ref. 21 for each of the fragments that are relaxed.

By relaxing the density of all frozen subsystems, fully variational subsystem DFT calculations can be performed. However, the main advantage of our flexible setup is the possibility to relax the density only for certain frozen subsystems. This allows the combination of the subsystem DFT approach as an efficient alternative to conventional KS-DFT calculations with the approximate frozen density treatment of large environments.

In Figure 1, an schematic overview of the different types of fragments that are possible and of the options that can be specified for each fragment is given. The implementation contains a number of approximate kinetic-energy functionals for the use in the FDE embedding potential, including the Thomas–Fermi functional and the widely used PW91k functional. The code for the evaluation of these functionals has been retained from the previous implementation of Wesolowski, as it was already suitable for the new setup.

For its flexible setup, our implementation makes use of modern object-oriented programming techniques. The code is written in Fortran90, and introduces abstract data types (ADTs) to represent

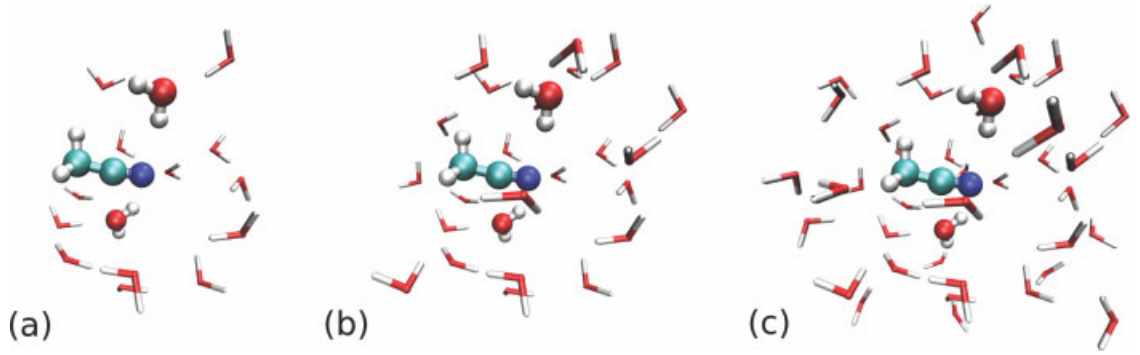

Figure 2. Structures of the acetonitrile–water clusters used in the test calculations. (a) acetonitrile surrounded by 15 water molecules, (b) acetonitrile surrounded by 25 water molecules, (c) acetonitrile surrounded by 40 water molecules. Graphics: VMD (Ref. 56).

fragments and their properties (like geometry, symmetry information, basis and fit function sets, molecular orbital coefficients, and fit coefficients). The use of these ADTs is not restricted to the FDE code, but they are now used throughout large parts of ADF. This restructured setup also facilitates the implementation of several extensions of the FDE formalism, such as the recently developed scheme for general subsystem TDDFT calculations on an arbitrary number of subsystems[45] that is based on the TDDFT generalization of FDE.[44]

Example of Application

To illustrate the capabilities of our new implementation, we present some test calculations from an ongoing project [Bulo et al., to be submitted], the description of the solvent effect on the nitrogen NMR chemical shift for acetonitrile in water. We have performed calculations on small clusters consisting of acetonitrile and 15, 25, and 40 water molecules, respectively. The structures have been taken from an arbitrary snapshot of a classical MD simulation. This simulation was performed with the NAMD high performance parallel molecular dynamics package[53] using a box of 30 Å in diameter, and the system was described using the CHARMM force field,[54] with standard TIP3P water molecules.[55] The water molecules included in the cluster are those nearest to the nitrogen atom of the acetonitrile. The studied clusters are shown in Figure 2.

In the calculations presented in the following, the NMR shieldings have been calculated using the extension of FDE to the calculation of magnetic properties,[24] and on the basis of the tests performed in ref. 24 the contributions of the induced current in the environment have been neglected. In all calculations, the TZ2P basis set from the ADF basis set library[49] has been used for acetonitrile as well as for water, and the exchange-correlation functional BP86, consisting of the exchange functional by Becke[57] and the correlation functional by Perdew,[58] has been employed throughout. The kinetic-energy functional PW91k[28] has been used to approximate the nonadditive kinetic-energy component of the FDE embedding potential.

In the FDE embedding calculations, the nonfrozen subsystem is formed by the acetonitrile molecule and the two closest water molecules. These are included in the nonfrozen subsystem to describe the hydrogen bonds to the nitrogen atom of acetonitrile accurately. The remaining water molecules are included in the calculation as frozen fragments, for which the density of the isolated molecule is used as initial frozen density. Since all solvent water molecules share the same geometry, this initial density only has to be calculated once and can then be used for all frozen water molecules.

The solvent shifts of the nitrogen NMR shielding calculated for the different clusters are given in Table 1. In all cases, the solvent shifts, i.e., the shift relative to the isolated acetonitrile molecule, are given.

For the cluster of acetonitrile and 15 water molecules, already the FDE calculation using the simplest sum-of-fragments (SumFrag) approximation for the frozen density, in which the frozen densities of the isolated molecules are used for all frozen fragments, leads to a solvent shift of 12.6 ppm. This is rather accurate compared to 14.0 ppm calculated in the conventional, supermolecular KS-DFT calculation. To improve this first approximation of the frozen density, our new implementation makes it possible to relax the electron densities of selected frozen fragments. In Table 1, the effect of relaxing the densities of some of the solvent water molecules is shown. In all cases, the densities were only relaxed in one freeze-in-thaw cycle, since we found that additional freeze-and-thaw cycles only have a minor effect on the calculated NMR shielding.

For the closest three water molecules, relaxing the density leads to an increase in the solvent shift of in total 1.2 ppm. For the water molecules that are further away, this effect is smaller. Relaxing the densities of five additional water molecules leads to an increase of only 0.9 ppm, and of the next five water molecules of only 0.7 ppm, i.e., the effect of relaxation decreases for water molecules that are further away from the nitrogen atom. However, as can be seen from Figure 2 also some of the water molecules at a larger distance from the nitrogen atom can be rather close to other parts of the acetonitrile molecule, so that it is not surprising that the relaxation of their density has an effect on the solvent shift that is rather large.

Table 1. Solvent Shifts $\Delta\sigma$ of the Nitrogen NMR Shielding in Acetonitrile–Water Clusters with 15, 25, and 40 Water Molecules, Respectively.

	15 H_2O $\Delta\sigma$ (ppm)		25 H_2O $\Delta\sigma$ (ppm)		40 H_2O $\Delta\sigma$ (ppm)	
Isolated	0.0		0.0		0.0	
SumFrag	12.6		11.9		11.8	
1 H_2O relaxed	12.9	+0.3	12.3	+0.4	11.9	+0.1
2 H_2O relaxed	13.3	+0.4	12.7	+0.4	12.4	+0.5
3 H_2O relaxed	13.7	+0.4	13.3	+0.6	13.1	+0.7
8 H_2O relaxed	14.6	+0.9	13.9	+0.6	14.0	+0.9
13 H_2O relaxed	15.3	+0.7	14.7	+0.8	14.7	+0.7
23 H_2O relaxed			15.2	+0.5	14.6	−0.1
38 H_2O relaxed					14.6	0.0
Supermolecule	14.0		13.1		12.5	

In the FDE calculations, the closest two water molecules have been included in the nonfrozen subsystem, for the remaining frozen fragments different approximations have been employed. For comparison, also the results of a conventional, supermolecular calculation are given. See text for details.

If the densities of all 13 frozen water molecules are relaxed, a solvent shift of 15.3 ppm is obtained, which is 1.3 ppm higher than the reference value from the supermolecular calculation. This remaining difference is due to the approximations introduced by the subsystem DFT treatment, in particular inaccuracies of the approximate kinetic-energy functional, differences in the basis set expansion,[32] and in the case of the calculation of NMR parameters also the neglect of the current dependence of the nonadditive kinetic energy and of the induced current in the frozen fragments.[24] By including more water molecules in the nonfrozen subsystem this error can be reduced, but this will also lead to an increase of the computational cost. The fact that the solvent shift calculated using the simple SumFrag approximation is nearly as close to the supermolecular reference value as in the case where all frozen densities are relaxed is due to an error cancellation between the error introduced by the approximate frozen density and the errors of the FDE treatment mentioned earlier.

When considering the large clusters containing 25 and 40 water molecules, respectively, the same trends as for the small cluster can be observed. While relaxing the densities of the water molecules close to the nitrogen atom has a larger effect, the effect of relaxing ten additional water molecules is only +0.5 ppm and −0.1 ppm in the clusters containing 25 and 40 water molecules, respectively. While for the relaxation of the water molecules closer to the acetonitrile, the effect of relaxation is roughly the same for all cluster sizes, for the relaxation of these ten water molecules this is not the case. This is because in the cluster containing 25 water molecules they are only polarized by the inner water molecules, while in the large cluster containing 40 water molecules, another layer of water molecules has been added that also polarizes the 10 water molecules in question. The effect of this outer layer is largest for the water molecules closest to it, i.e., further away from the acetonitrile, while its effect on the inner water molecules is rather small. In the cluster containing 40 water molecules, the effect of relaxing the densities of the additional outer layer of 25 water molecules is negligible.

For both clusters, the difference between the supermolecular reference value and the solvent shift calculated when the densities of all frozen water molecules are relaxed are approximately 2 ppm. It should be noted that this error is of similar size as other errors that appear in the conventional KS-DFT calculation of NMR shieldings, such as basis set effects and inaccuracies in the exchange-correlation functional. As mentioned above, in the case that fewer frozen water molecules are relaxed, the error introduced by the FDE treatment, in particular the use of an approximate kinetic-energy functional, are (partly) canceled by the error caused by the use of a more approximate frozen density.

In Table 2, the wall clock times required for the calculations discussed above on 8 dual processor nodes of an Intel Xeon 3.4 GHz cluster are given. These timings show for the three clusters a slight increase in the required computer time when a larger number of frozen fragments are relaxed. This is due to the additional freeze-and-thaw cycles needed in this case. Going to a larger cluster, the required time increases approximately linear with the number of water molecules included, which is due to the increased size of the numerical integration grid as well as the additional effort for constructing the larger frozen density. Because of this linear scaling, the FDE calculations are significantly more efficient compared to the supermolecular calculation of the NMR shielding, especially for larger clusters. A large part of this difference is caused by the fact that in the FDE case, the calculation of the NMR shielding can be performed for the much smaller nonfrozen system only, while including the effect of the frozen environment in the FDE embedding potential.

Table 2. Wall Clock Time (in Minutes) Required for the Calculation of the Nitrogen NMR Shielding in Acetonitrile–Water Clusters with 15, 25, and 40 Water Molecules, Respectively, on 8 Dual Processor Nodes of an Intel Xeon 3.4 GHz Cluster, Using Different Approximations for the Frozen Density (see text for details).

	15 H_2O	25 H_2O	40 H_2O
Isolated	0.4	0.4	0.4
SumFrag	1.7	2.1	2.9
1 H_2O relaxed	2.6	3.1	4.3
2 H_2O relaxed	2.8	3.6	5.0
3 H_2O relaxed	3.0	3.8	5.0
8 H_2O relaxed	3.6	5.2	6.2
13 H_2O relaxed	4.0	5.3	7.2
23 H_2O relaxed		7.1	9.4
38 H_2O relaxed			12.8
Supermolecule	8.5	29.8	103.5

The presented test calculations demonstrate how the approximate frozen density can be improved by relaxing the densities of frozen fragments. Especially for solvent molecules close to the nonfrozen subsystem, this will be important to obtain accurate results.[21,22] However, for solvent molecules that are further away from the nonfrozen subsystem the effect of relaxation is rather small. Therefore, it is possible to restrict the number of frozen fragments that are relaxed and to avoid the increased computational effort caused by relaxing the densities of all frozen fragments. This will be particularly useful in practical applications requiring calculations for hundreds of snapshots and the inclusion of a large number of solvent molecules. On the basis of our tests, we chose to relax the densities of 13 solvent water molecules, in addition to the two water molecules that are included in the nonfrozen subsystem. However, the accurate description of the nitrogen NMR chemical shift of acetonitrile in water will require calculations on a large number for snapshots from MD simulations. This requires more thorough tests than those presented here, and a detailed study will be presented elsewhere [Bulo et al., to be submitted].

The solvent shifts of the nitrogen NMR shielding calculated in FDE calculations using this setup (i.e., two water molecules are nonfrozen, and the densities of 13 additional water molecules are relaxed) including up to 250 water molecules are shown in Figure 3. It can be seen that up to approximately 100 water molecules, the solvent shift shows a rather irregular behavior, while adding further water molecules leads to a smooth increase of the solvent shift. The observation that the water molecules 50–75 lead to a larger change of the solvent shifts than water molecules 25–50 is due to the geometries of the investigated clusters. Since the water molecules are chosen according to their distance from the nitrogen atom of the acetonitrile molecule, the water molecules 50–75 include several water molecules close to methyl group of acetonitrile, which

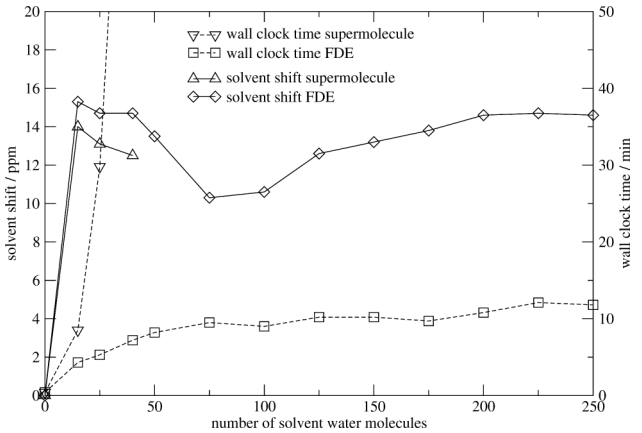

Figure 3. Solvent shift on the nitrogen NMR shielding of acetonitrile in water (solid line), calculated including solvent shells of different size. The results of the FDE calculations (squares/diamonds) and for small solvent shells of supermolecule calculations (triangles) are given. In addition, also the wall clock time (dashed line) required on 8 dual processor nodes of an Intel Xeon 3.4 GHz cluster are shown. See text for details.

influence its electronic structure significantly. Only after approximately 100 solvent water molecules have been included, the acetonitrile is completely surrounded by solvent molecules and the effect of the addition of further solvent molecules becomes more regular.

As can be seen from Figure 3, approximately 200 solvent water molecules have to be included to obtain a solvent shift that is converged with respect to the size of the solvent shell. The required wall clock times that are included in Figure 3 show that this is easily possible in the FDE calculations. While for solvent shells up to 50 atoms the computer time increases approximately linearly, for larger solvent shells the time required for the FDE calculation is almost constant. In contrast, because of their unfavorable scaling, the conventional supermolecular KS-DFT calculations become infeasible already for rather small solvent shells.

Conclusions

We have presented a new implementation of the FDE scheme, which allows both a frozen density treatment using an approximate environment density as well as a subsystem DFT treatment, in which the densities of all subsystems are determined. In addition, intermediate treatments are possible, in which only the densities of a few subsystems are relaxed, in the presence of a larger frozen environment.

This flexible scheme offers several new possibilities for the multilevel description of environment effects. The partial relaxation of the electron density of the environment makes it possible to include not only the electronic coupling of the environment with the nonfrozen subsystem, but to include the polarization of the environment due to the nonfrozen subsystem as well. This results in a very accurate description of the coupling between different regions described at the QM level, in contrast to other popular QM/QM methods[5,10–12] that only include a mechanical coupling between the different regions.

As we show for the NMR chemical shift of acetonitrile in water, this flexible FDE scheme can be employed to improve the FDE treatment using an approximate environment density. By relaxing the electron densities of some solvent molecules that are close to the subsystem of interest, it is possible to adjust the accuracy of the description of the environment to the degree needed. At the same time, the total time of the computation only increases moderately. In particular, the time needed for the calculation of the NMR chemical shift does not increase, since it can be performed for the nonfrozen subsystem only.

Because of the numerical integration scheme used, our FDE implementation is very efficient, in particular for large frozen environments. It allows the treatment of environments consisting of hundreds of atoms, which makes it an attractive method for modeling large systems such as solvent environments or biological systems.

The FDE implementation described here is included in the 2007 release of the ADF program package. The FDE scheme can be combined with the calculation of several molecular properties that are available in ADF. Currently, properties that depend directly on the electron density (such as dipole and quadrupole moments), electronic excitation energies and polarizabilities can be calculated, as well as NMR shieldings and ESR hyperfine coupling constants. The extension to other properties, such as energy gradients, vibrational frequencies, and NMR spin–spin coupling constants is currently in progress. The FDE scheme can be combined with additional, more approximate descriptions of environments that are present in ADF, like continuum solvation models or different QM/MM schemes.

Our flexible setup will make several extensions of the implementation possible. An extension of the implementation to the calculation of excited states, that uses the recently proposed protocol for subsystem-TDDFT calculations with an arbitrary number of subsystems,[45] is currently being integrated into the new FDE implementation and will be included in a future release. First test applications of this methods have already shown that it will be very useful for the description of excitonic couplings between different subsystem.

In addition, we are working on an extension to molecular dynamics and on coupling our implementation to *ab initio* codes to allow the treatment of individual subsystems using wave function based methods, similar to the *ab initio*-in-DFT embedding scheme by Carter and co-workers.[59–61]

Acknowledgments

The authors thank Tomasz Wesolowski (University of Geneva) for stimulating discussions and for providing the first implementation of the FDE scheme in ADF. The authors further thank Rosa Bulo (Vrije Universiteit Amsterdam) for providing the example application and for helpful comments and discussions. The authors gratefully acknowledge computer time provided by the Dutch National Computing Facilities (NCF).

References

1. Schöneboom, J. C.; Neese, F.; Thiel, W. J Am Chem Soc 2005, 127, 5840.
2. Leenders, E. J. M.; Guidoni, L.; Röthlisberger, U.; Vreede, J.; Bolhuis, P. G.; Meijer, E. J. J Phys Chem B 2007, 111, 3765.
3. Prabhakar, R.; Vreven, T.; Frisch, M. J.; Morokuma, K.; Musaev, D. G. J Phys Chem B 2006, 110, 13608.
4. Olsson, M. H. M.; Hong, G.; Warshel, A. J Am Chem Soc 2003, 125, 5025.
5. Humbel, S.; Sieber, S.; Morokuma, K. J Chem Phys 1996, 105, 1959.
6. Warshel, A.; Levitt, M. J Mol Biol 1976, 103, 227.
7. Gao, J. In Reviews in Computational Chemistry, Vol. 7; Lipkowitz, K. B.; Boyd, D. B., Eds. VCH: New York, 1995; pp. 119–185.
8. Senn, H. M.; Thiel, W. Top Curr Chem 2007, 268, 173.
9. Bakowies, D.; Thiel, W. J Phys Chem 1996, 100, 10580.
10. Svensson, M.; Humbel, S.; Froese, R.; Matsubara, T.; Sieber, S.; Morokuma, K. J Phys Chem 1996, 100, 19357.
11. Vreven, T.; Morokuma, K. J Comput Chem 2000, 21, 1419.
12. Swart, M.; Bickelhaupt, F. M. J Comput Chem, in press, DOI: 10.1002/jcc.20834.
13. Sherwood, P. In Modern Methods and Algorithms of Quantum Computing, Vol. 1: NIC series; Grotendorst, J., Ed. John von Neumann Institute for Computing: Jülich, 2000; pp. 257–277.
14. Laio, A.; VandeVondele, J.; Rothlisberger, U. J Chem Phys 2002, 116, 6941.
15. Kongsted, J.; Osted, A.; Mikkelsen, K. V.; Christiansen, O. J Mol Struct.: THEOCHEM 2003, 632, 207.
16. Jensen, L.; van Duijnen, P. Th.; Snijders, J. G. J Chem Phys 2003, 118, 514.
17. Jensen, L.; van Duijnen, P. Th.; Snijders, J. G. J Chem Phys 2003, 119, 3800.
18. Wesolowski, T. A.; Warshel, A. J Phys Chem 1993, 97, 8050.
19. Wesolowski, T. A. In Computational Chemistry: Reviews of Current Trends, Vol. 10; Leszczynski, J., Ed.; World Scientific: Singapore, 2006.
20. Neugebauer, J.; Louwerse, M. J.; Baerends, E. J.; Wesolowski, T. A. J Chem Phys 2005, 122, 094115.
21. Neugebauer, J.; Jacob, Ch. R.; Wesolowski, T. A.; Baerends, E. J. J Phys Chem A 2005, 109, 7805.
22. Jacob, Ch. R.; Neugebauer, J.; Jensen, L.; Visscher, L. Phys Chem Chem Phys 2006, 8, 2349.
23. Neugebauer, J.; Louwerse, M. J.; Belanzoni, P.; Wesolowski, T. A.; Baerends, E. J. J Chem Phys 2005, 123, 114101.
24. Jacob, Ch. R.; Visscher, L. J Chem Phys 2006, 125, 194104.
25. Neugebauer, J.; Baerends, E. J. J Phys Chem A 2006, 110, 8786.
26. Štrajbl, M.; Hong, G.; Warshel, A. J Phys Chem B 2002, 106, 13333.
27. Cortona, P. Phys Rev B 1991, 44, 8454.
28. Lembarki, A.; Chermette, H. Phys Rev A 1994, 50, 5328.
29. Wesolowski, T. A. J Chem Phys 1997, 106, 8516.
30. Jacob, Ch. R.; Wesolowski, T. A.; Visscher, L. J Chem Phys 2005, 123, 174104.
31. Jacob, Ch. R.; Beyhan, S. M.; Visscher, L. J Chem Phys 2007, 126, 234116.
32. Wesolowski, T. A.; Weber, J. Chem Phys Lett 1996, 248, 71.
33. Cortona, P. Phys Rev B 1992, 46, 2008.
34. Cortona, P.; Villafiorita Monteleone, A. J Phys: Condens Matter 1996, 8, 8983.
35. Cortona, P.; Villafiorita Monteleone, A.; Becker, P. Int J Quantum Chem 1995, 56, 831.
36. Mei, W. N.; Boyer, L. L.; Mehl, M. J.; Ossowski, M. M.; Stokes, H. T. Phys Rev B 2000, 61, 11425.
37. Ossowski, M. M.; Boyer, L. L.; Mehl, M. J.; Stokes, H. T. Phys Rev B 2002, 66, 224302.
38. "CP2K", The CP2K developers group, URL: http://cp2k.berlios.de, 2007.
39. VandeVondele, J.; Krack, M.; Mohamed, F.; Parrinello, M.; Chassaing, T.; Hutter, J. Comput Phys Commun 2005, 167, 103.
40. Iannuzzi, M.; Kirchner, B.; Hutter, J. Chem Phys Lett 2006, 421, 16.
41. Shimojo, F.; Kalia, R. K.; Nakano, A.; Vashishta, P. Comput Phys Commun 2005, 167, 151.
42. Vashishta, P.; Kalia, R.; Nakano, A. J Phys Chem B 2006, 110, 3727.
43. Wesolowski, T.; Warshel, A. J Phys Chem 1994, 98, 5183.
44. Casida, M. E.; Wesolowski, T. A. Int J Quantum Chem 2004, 96, 577.
45. Neugebauer, J. J Chem Phys 2007, 126, 134116.
46. Köster, A. M.; Calaminici, P.; Casida, M. E.; Flores-Moreno, R.; Geudtner, G.; Goursot, A.; Heine, T.; Ipatov, A.; Janetzko, F.; del Campo, J. M.; Patchkovskii, S.; Reveles, J. U.; Salahub, D. R.; Vela, A. "deMon2k", URL: http://www.demon-software.com, 2006.
47. Dulak, M.; Wesolowski, T. A. Int J Quantum Chem 2004, 101, 543.
48. Dułak, M.; Kamiński, J. W.; Wesołowski, T. A. J Chem Theory Comput 2007, 3, 735.
49. "ADF, Amsterdam density functional program", Theoretical Chemistry, Vrije Universiteit Amsterdam, URL: http://www.scm.com, 2007.
50. te Velde, G.; Bickelhaupt, F. M.; Baerends, E. J.; Fonseca Guerra, C.; van Gisbergen, S. J. A.; Snijders, J. G.; Ziegler, T. J Comput Chem 2001, 22, 931.
51. Wesolowski, T. A. J Am Chem Soc 2004, 126, 11444.
52. Bickelhaupt, F. M.; Baerends, E. J. In Reviews in Computational Chemistry, Vol. 15; Lipkowitz, K. B.; Boyd, D. B., Eds.; Wiley-VCH: New York, 2000; pp. 1–86.
53. Kalé, L.; Skeel, R.; Bhandarkar, M.; Brunner, R.; Gursoy, A.; Krawetz, N.; Phillips, J.; Shinozaki, A.; Varadarajan, K.; Schulten, K. J Comput Phys 1999, 151, 283.
54. MacKerell, A. D., Jr.; Brooks, B.; Brooks, C. L., III; Nilsson, L.; Roux, B.; Won, Y.; Karplus, M. In The Encyclopedia of Computational Chemistry, Vol. 1; Schleyer, P. v. R., Ed. Wiley: Chichester, 1998; pp. 271–277.
55. Jorgensen, W. L.; Chandrasekhar, J.; Madura, J. D.; Impey, R. W.; Klein, M. L. J Chem Phys 1983, 79, 926.
56. Humphrey, W.; Dalke, A.; Schulten, K. J Mol Graphics 1996, 14, 33.
57. Becke, A. D. Phys Rev A 1988, 38, 3098.
58. Perdew, J. P. Phys Rev B 1986, 33, 8822.
59. Govind, N.; Wang, Y. A.; Carter, E. A. J Chem Phys 1999, 110, 7677.
60. Klüner, T.; Govind, N.; Wang, Y. A.; Carter, E. A. Phys Rev Lett 2001, 86, 5954.
61. Huang, P.; Carter, E. A. J Chem Phys 2006, 125, 084102.